Growth, Distribution, and Photosynthesis of Chlamydomonas Reinhardtii in 3D Hydrogels

Oh, Jeong Joo; Ammu, Satya; Vriend, Vivian Dorine; Kieffer, Roland; Kleiner, Friedrich Hans; Balasubramanian, Srikkanth; Karana, Elvin; Masania, Kunal; Aubin-Tam, Marie Eve

DOI
10.1002/adma.202305505

Publication date
2023

Document Version
Final published version

Published in
Advanced Materials

Citation (APA)
Oh, J. J., Ammu, S., Vriend, V. D., Kieffer, R., Kleiner, F. H., Balasubramanian, S., Karana, E., Masania, K., & Aubin-Tam, M. E. (2023). Growth, Distribution, and Photosynthesis of Chlamydomonas Reinhardtii in 3D Hydrogels. *Advanced Materials*, *36*(2), Article 2305505. https://doi.org/10.1002/adma.202305505

ADVANCED MATERIALS
www.advmat.de

Growth, Distribution, and Photosynthesis of *Chlamydomonas Reinhardtii* in 3D Hydrogels

Jeong-Joo Oh, Satya Ammu, Vivian Dorine Vriend, Roland Kieffer, Friedrich Hans Kleiner, Srikkanth Balasubramanian, Elvin Karana, Kunal Masania, and Marie-Eve Aubin-Tam**

Engineered living materials (ELMs) are a novel class of functional materials that typically feature spatial confinement of living components within an inert polymer matrix to recreate biological functions. Understanding the growth and spatial configuration of cellular populations within a matrix is crucial to predicting and improving their responsive potential and functionality. Here, this work investigates the growth, spatial distribution, and photosynthetic productivity of eukaryotic microalga *Chlamydomonas reinhardtii (C. reinhardtii)* in three-dimensionally shaped hydrogels in dependence of geometry and size. The embedded *C. reinhardtii* cells photosynthesize and form confined cell clusters, which grow faster when located close to the ELM periphery due to favorable gas exchange and light conditions. Taking advantage of location-specific growth patterns, this work successfully designs and prints photosynthetic ELMs with increased CO_2 capturing rate, featuring high surface to volume ratio. This strategy to control cell growth for higher productivity of ELMs resembles the already established adaptations found in multicellular plant leaves.

1. Introduction

Engineered living materials (ELMs) integrate living organisms as active components within natural or synthetic matrices to create life-like functions[1] such as metabolite production, stimuli-responsiveness, programmable development and growth, and self-repair.[2–4] These biohybrid materials usually require that the living organisms grow and function properly while being spatially confined within an associative matrix. The matrix needs to provide a favorable environment for growth, while allowing sufficient mass transfer of gas and nutrients. For more predictable, highly functional ELMs with increased longevity, it is crucial to understand the cell growth within matrices, and to identify the environmental factors important for cells' productivity and function. Recent studies of bacteria and yeasts confined in hydrogels showed that cells formed nonmotile spherical clusters primarily localized in the periphery of hydrogels.[5,6] These observations suggest that simply increasing the total volume of ELMs would not necessarily lead to higher functionality/productivity.

Photosynthetic microorganisms can be integrated into polymeric matrices to form ELMs with plant-like qualities,[7–17] allowing them to photosynthesize and thus to provide a localized O_2 source[12,15] and/or CO_2 sink. The high tolerance of many microalgae to abiotic stress factors such as temperature, pH, or osmotic stress broaden the spectrum of potential applications for photosynthetic ELMs. Based on these properties, microalgal ELMs show great promise for generating bioelectricity,[14] oxygenating mammalian tissues in biomedical applications,[15] improving air and water quality,[7,9,16] and granting photoresponsive/photoadaptive functions to materials. The current research on fabrication of microalgal ELMs has so far focused on formulation of hydrogel,[10] viability of embedded cells,[8,10,15] and O_2 production capacity in dependence of time.[7,9] However, fundamental understanding on how microalgae cells spatially localize and grow within matrices is still in its infancy, which has been the major obstacle to predict and intensify the functionality of these photosynthetic ELMs.

Here, we investigate the growth, spatial distribution, and photosynthetic productivity of eukaryotic microalga *Chlamydomonas reinhardtii* (*C. reinhardtii*) within a mechanically stable 3D printed hydrogel-based ELM over time (**Figure 1**). By regulating geometry and tuning hydrogel composition, we identify important factors that impact the spatial localization of embedded cells. Based on these factors, and inspired by plant leaves, we successfully

J.-J. Oh, V. D. Vriend, R. Kieffer, F. H. Kleiner, S. Balasubramanian, M.-E. Aubin-Tam
Department of Bionanoscience
Kavli Institute of Nanoscience
Delft University of Technology
Van der Maasweg 9, Delft 2629 HZ, The Netherlands
E-mail: m.e.aubin-tam@tudelft.nl

S. Ammu, K. Masania
Shaping Matter Lab
Faculty of Aerospace Engineering
Delft University of Technology
Kluyverweg 1, Delft 2629 HS, The Netherlands
E-mail: k.masania@tudelft.nl

V. D. Vriend, S. Balasubramanian, E. Karana
Department of Sustainable Design Engineering
Faculty of Industrial Design Engineering
Delft University of Technology
Landbergstraat 15, Delft 2628 CE, The Netherlands

The ORCID identification number(s) for the author(s) of this article can be found under https://doi.org/10.1002/adma.202305505

DOI: 10.1002/adma.202305505

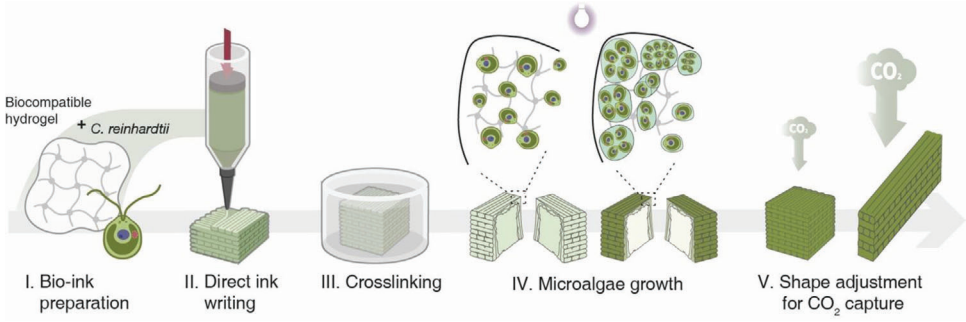

Figure 1. Schematic diagram exhibiting the individual steps from I) biocompatible ink formulation containing eukaryotic microalga *Chlamydomonas reinhardtii* (*C. reinhardtii*), II) three-dimensional shaping of the engineered living materials (ELM) based on a direct ink writing method, III) cross-linking for mechanical stability, IV) characterization of cell growth and spatial distribution of microalgae in different light regimes, and V) shape adjustment of ELMs for higher photosynthetic activity.

adjust our gel architecture to accommodate the needs of the cells, allowing higher photosynthetic activity.

2. Results

2.1. Shaping *C. reinhardtii*-Laden Bioprints

Shaping of ELMs with 3D printing allows spatial arrangement of a bioink into favorable cell growth conditions, thereby increasing the ELM functionality in a manner that is difficult to achieve with molding approaches.[12,15] *Chlamydomonas reinhardtii* cells mixed with κ-carrageenan, sodium alginate, agar, and cellulose-based thickener were 3D printed by direct extrusion and deposition in a layer-by-layer fashion. A similar ink composition enabled the printing of mycelium-based ELM structures that are not limited in height,[18] as opposed to most alginate-based printing approaches.[17,19] Ideally, the 3D printed matrix should exhibit enough resistance to capillarity- and gravity-driven physical deformation for self-support and should be sufficiently strong and stiff to maintain structural integrity while being manipulated after the printing process. Such manipulation was not possible with the original ink composition,[18] which harnessed hyphal growth to introduce structural integrity to the hydrogel. We therefore first proceeded by developing an approach to mechanically strengthen the matrix through cross-linking.

Sodium alginate was included in the ink, aiming to achieve higher mechanical robustness, due to the ability of alginate to form a hydrogel when cross-linked with Ca^{2+} ions. We investigated whether Ca^{2+} diffusion into the alginate-containing prints (without algae) would lead to higher mechanical stiffness of ELMs (**Figure 2**a). The optimal cross-linking conditions were determined with a comparison of storage moduli (G') of prints immersed into solutions with varying Ca^{2+} molarity (0.1–0.5 M) for different durations (5 and 60 min). By immersing the prints for 5 min at respective concentrations, the storage moduli were found to plateau at a Ca^{2+} concentration of 0.2 M (Figure 2b). Immersing prints for 5 and 60 min into 0.2 M Ca^{2+} solution provided similar mechanical properties (Figure 2c). Thus, soaking prints into 0.2 M Ca^{2+} solution for 5 min was set as the optimal cross-linking procedure, where the yield point significantly increased from 426 Pa to 6.1 kPa after cross-linking (Figure 2d). Although aging prints for 2 weeks without controlled Ca^{2+} cross-linking also results in an increased yield point, the yield point is lower (4.6 kPa) (Figure 2e). These results show the value of Ca^{2+} alginate cross-linking to achieve higher mechanical robustness within a short time (Video S1, Supporting Information).

A reproducible "bioink" with a cell density of 6.67×10^5 cells g^{-1} within the alginate-containing ink was prepared to fabricate microalgal ELMs (Figure S1, Supporting Information). Embedded cells potentially affect the rheology of the ink and mechanical properties of prints.[20–23] Further, the embedded cells represent physical obstacles which may limit interaction between matrix components or interfere with cross-linking of components and vary the mechanical stability.[24,25] To quantify the possible effects of cell embedding, the rheological behavior of the bioink and the mechanical stability of cross-linked bioprints were investigated.

The rheological behavior of the bioink was studied with focus on flow behavior and recovery of viscoelasticity. The incorporation of *C. reinhardtii* into the ink did not considerably affect the flow behavior. As shown in Figure 2d, ink with and without living cells both displayed shear-thinning behaviors and had similar yield stress values (426 Pa without cells, 413 Pa with cells). The elastic recovery of the ink with and without algae after yield was measured using an oscillation-rotation and oscillation test. Rotational shear was applied to simulate the high extrusion force, whereas the oscillatory shear measurement was applied to quantify the storage modulus of the bioink before and after yield. After incorporating *C. reinhardtii* cells, the properties of viscoelasticity recovery were not changed (Figure 2f). Both prints showed instantaneous elastic recovery within seconds, meaning that filaments of both inks can prevent flow-induced distortion after the deposition. These results confirm that the bioink has similar rheological properties as the cell-free ink. At 0.03 wt%, the low weight fraction of cells in bioink did not influence the yield stress (Figure S1, Supporting Information).

Likewise, the mechanical stability was unaffected by the incorporation of living cells. Soaking the cell-containing bioprints in Ca^{2+} solution significantly increased the yield point from 413 Pa to 5.7 kPa (Figure 2d), which is similar to cell-free prints. In addition, aging of cross-linked bioprints for 2 weeks further increases the yield point to 12 kPa (Figure 2g). These observations inform us that the shaping and cross-linking approach is promising, and the microalgal ELMs demonstrate more mechanical robustness over time.

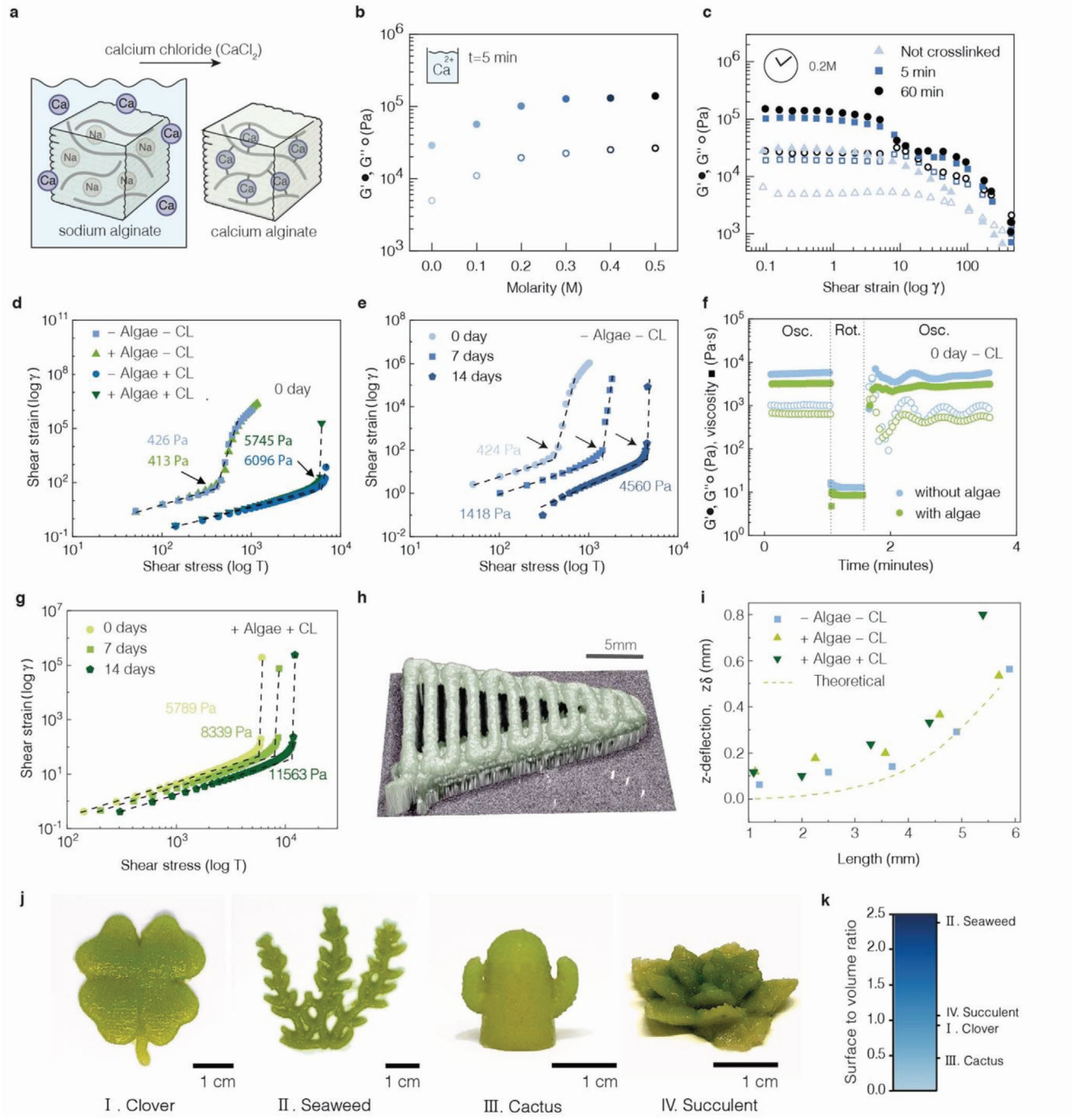

Figure 2. Rheological behavior of *Chlamydomonas reinhardtii* (*C. reinhardtii*) laden bioprints. a) Schematics displaying the cross-linking of prints using calcium chloride for transition of sodium alginate to calcium alginate. b) Effects of Ca^{2+} molarity on the storage (G') and loss moduli (G'') of the print without microalgae. c) Influence of cross-linking time on the storage (G') and loss moduli (G'') of the print without microalgae as a function of oscillatory shear strain. d) Flow behavior of 0-day old prints depending on cross-linking and microalgae integration. e) Flow behavior changes of prints without microalgae nor cross-linking over 2 weeks. Black arrows with numerical values in (d) and (e) indicate the yield points above which physical deformation occurs. f) Elastic recovery of prints (not cross-linked) depending on microalgae integration. g) Yield stress of cross-linked cell-containing bioprints, 0, 7, and 14 days after printing and cross-linking. h) Bridging ability of the *C. reinhardtii* laden prints (not cross-linked). i) Measured and calculated deflection (δ_{zmax}) of the bridging filaments as a function of their spanning length. j) 3D microalgal engineered living materials (ELMs) in the shape of a cactus, clover, aloe, and seaweed, 14 days after incubation under autotrophic conditions. k) Theoretical surface to volume ratio of microalgal ELMs. CL indicates Ca^{2+} cross-linking of hydrogel.

Complex geometries such as grid-like or hollow structures can enable increased functionality for ELMs.[18,26] These features require shape fidelity of filaments over a supporting structure. To quantify the shape fidelity, the bridging capability of the *C. reinhardtii*-laden printed hydrogel was investigated.[27] A support structure with increasingly long spanning elements was printed, as shown in Figure 2h. The extent of sagging as a function of the length of the filament was determined by measuring z-deflection using optical profilometry.[27] The deflection of the printed filaments scales with the spanning length, as shown in Figure 2i. The filament could be bridged up to 3.5 mm with less than 0.2 mm of tolerable sagging, suggesting complex geometries within a limited bridging length could be formed.

The achieved rheological properties and shape fidelity of the bioink enable the fabrication of various macroscopic 3D geometries of ELMs with complex features (Figure 2j). We printed open architectures which provide a 3D environment for the growth of algae throughout the hydrogel into functional materials benefiting from high surface area. The shaping capabilities of 3D printing can be exploited to manufacture geometries that match the functional requirements of specific scenarios. The yield stress of the ink is an important parameter in the shaping; and cross-linking the ELM after printing increased the yield stress by one order of magnitude. This allows difficult shapes such as the overhanging arms of the cactus structure.

Flat prints with small protrusions of less than 5 mm (for seaweed shape) were prepared without flow-induced distortion after extrusion. The high yield points of the cross-linked bioink enable standing shapes with hanging elements, as exemplified by the arms of the cactus and the floating leaves of succulent plant. Using computational approach, the volume and surface area of the ELM structures were compared (Figure 2k). We note that the highly branched nature of the seaweed geometry demonstrates the highest surface to volume ratio, at almost 5.5 times higher than the cactus structure.

2.2. Growth of Embedded *C. reinhardtii* Inside Hydrogels

We chose a 1 cm^3 cube-shaped ELM as a model to characterize the growth of *C. reinhardtii* cells within hydrogels. The cubes were incubated under autotrophic conditions (i.e., without another carbon source than CO_2 from the atmosphere) and cell growth was monitored over time by visual inspection (**Figure 3**a). At day 0, bioprints displayed a white color, mainly representing the raw Ca^{2+} cross-linked hydrogels. After 3 days of incubation, the surface of bioprints started to display a faint green indicating growth of microalgae. Continuous growth over the following 14 days led to a darker green. After 14 days, no further change in color was observed for the next 35 days (Figure S2, Supporting Information). Examination of cross-sectional cuts of bioprints revealed that the growth of microalgae mostly occurred in a thin layer of 1–2 mm below the outer periphery of the cube (Figure 3a), in which most cells stay alive beyond 14 days (Figure S3, Supporting Information). Confocal scanning microscopic imaging showed that *C. reinhardtii* cells were nonmotile and form individual colonies within the hydrogel, and that each colony originates from a single cell rather than being the result of aggregation of cells (Figure S4, Supporting Information). Light microscopic images revealed the presence of a thin membrane-like structure at the periphery of individual colonies, suggesting that cells entered the palmelloid stage[28] (Figure 3b,c; Figure S5, Supporting Information). In liquid culture, the palmelloid stage is formed in response to various stresses.[29,30] *Chlamydomonas reinhardtii* were also found to be in a state consistent with palmelloids (no flagella, cluster formation) when embedded in other hydrogel systems.[7,17,31,32] Cells within our hydrogel are likely to form clusters as a passive result of cell division within a confined environment, although we cannot exclude palmelloids being induced (partly) by other stress factors.[28–30] Printed 1 cm^3 cubes immersed in Tris minimal media also showed similar growth to those observed in air-exposed cubes, and individual colonies formed within the hydrogel (Figure S6, Supporting Information). Interestingly, submerging the 14-day old ELM placed in air in Tris minimal medium induced the algae cells to flagellate, regain their motility, and populate the surrounding medium (Video S2, Supporting Information).

The gradual decrease of "greenness" toward the center of the cube warranted further investigation of the location-specific growth of embedded *C. reinhardtii* cells (Figure 3a). The cube was divided into four zones ranging from topical periphery to the center of the cube (Supporting Information). In each zone, the number of colonies was counted, and their volume was calculated assuming a spherical shape for the colonies. At day 0, an average of 40 colonies were counted in each zone (Figure 3d). Within 3 days, the number of colonies below 1.25 mm decreased to fewer than 12 and remained in this range until the end of the experiment. In contrast, the number of colonies within 1.25 mm from the surface steadily increased, reaching 156 ± 20 at day 14. Simultaneously, with increasing depth, the volume of colonies decreased (Figure 3e). At day 0, the average calculated colony volume was approximately 358 μm^3, which represents a volume that would correspond to an individual *C. reinhardtii* cell.[33] In the periphery, the average volume of colonies increased gradually to 5209 μm^3 within 14 days, while growth in the volume of colonies within increased depth was smaller. Notably, up to a depth of 3.75 mm, a few colonies were able to grow in volume at 14 days (Figure 3e). These results imply that the colonies close to the periphery tend to survive and grow as nonmotile clusters while cells near the center did not grow after 3 days, which is in correlation with the color shift of the green cube periphery to the white cube center.

2.3. Exploring the Limiting Factors for Embedded *C. Reinhardtii* Cell Growth

To explore whether the reduced autotrophic growth of algae in the center of the ELM cube is due to limited penetration of light and/or CO_2, ELM shapes with different thicknesses or improved gas exchange were tested and colony growth was examined. 2 mm thick plate-shaped ELMs were deposited on a solid plastic surface to prevent air transfer at the bottom (**Figure 4**a), and placed under LEDs mainly composed of blue (453 nm) and red (631 nm) light. A light sensor placed below the ELM-plate measured light transmission across 2 mm of ELM material. In 0-day-old ELM-plates, the measured light intensity was reduced from 6.7 to 2.5 $\mu mol\ m^{-2}\ s^{-1}$ at 453 nm, and from 13.3 to 7.7 $\mu mol\ m^{-2}\ s^{-1}$ at 631 nm, accounting a 62% and 43%

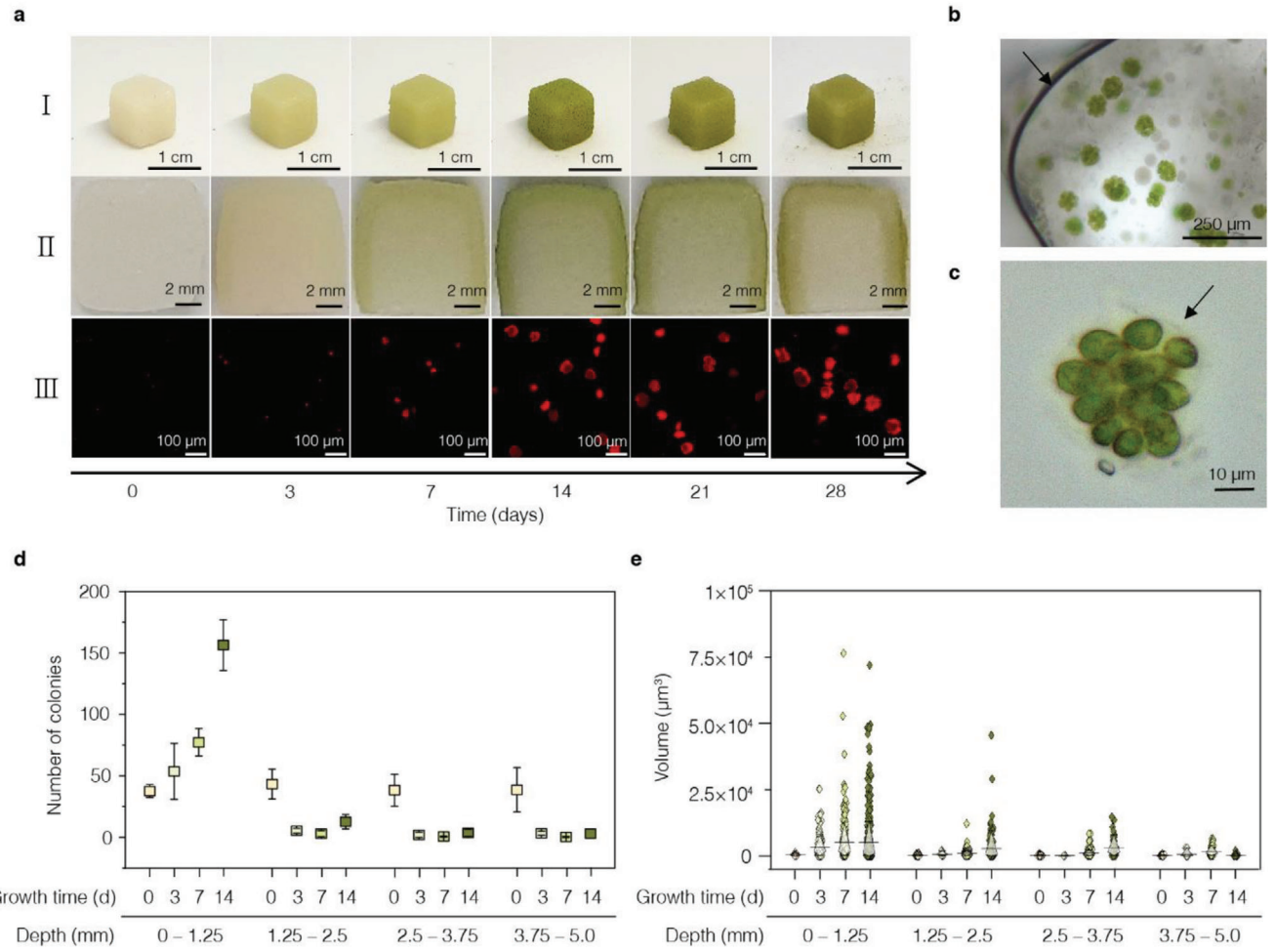

Figure 3. Growth and spatial distribution of embedded *Chlamydomonas reinhardtii* (*C. reinhardtii*) cells in cube-shaped engineered living materials (ELMs) ($V = 1\ cm^3$). a) Time-series of ELM-maturation during 28 days under autotrophic conditions. I) Macroscopic images of the ELMs. II) Images of cross-sections of respective ELMs. III) Confocal microscopic images showing chlorophyll autofluorescence of embedded cells approximately 100 µm below the surface of the ELM. b) Light microscopic images of embedded cells around the outer periphery (black arrow) of a 14-day old cube, showing cells switched to the palmelloid life stage. c) Light microscopic image of an individual cluster surrounded by a transparent extracellular matrix (black arrow). d) The average number of colonies per 1.56 mm^2 area in relation to incubation time and distance to the cube surface (3 cubes per time point, whiskers extend to standard deviations). e) Volume of colonies in relation to incubation time and distance to the cube surface. In (e), three cubes were used for the distributions, diamond boxes indicate 10 and 90 percentile values, and the horizontal lines in the middle indicate the mean.

reduction, respectively (Figure 4b). *Chlamydomonas reinhardtii* was shown to be able to grow at similar light regimes in where a total intensity is sufficient for growth of *C. reinhardtii* cells.[34] After 14 days, light attenuation was increased to approximately 70% and 50%, respectively (Figure S7), likely from cell growth at the outer periphery. Despite sufficient light transmission to inner layers, no significant increase in colony volume and greenness was observed at a depth between 1.5 and 2 mm after 14 days (Figure 4c). This suggests that light availability is not the only limiting growth factor in this layer.

Besides light attenuation, cells located in deeper layers may also face limited CO_2 availability. To investigate the role of CO_2 availability on growth of embedded algae, hollow ELM-hemispheres ("igloo" shaped) of 2 mm thickness with variable medium composition were designed (Figure 4d). ELM-hemispheres showed similar light penetration properties as ELM-plates of same thickness (Figure S7, Supporting Information). The ELM-hemispheres were placed on a plasticware with two rectangular shaped holes (area: 2 × 3 mm) that allowed gas to enter and exit the inner space of the hemisphere. After 14 days of incubation, both the outer and inner surface displayed significant growth of colonies (Figure 4e). However, colonies located in the intermediate depth of 0.5–1.0 mm from the surface showed less increase in volume compared to the ones in peripheries. These findings indicate that improved gas exchange indeed improves cell proliferation. To test this further, the experiment was repeated with ELM-hemispheres of identical architecture but containing an additional carbon source (acetate) from the Tris-acetate-phosphorous (TAP) medium. Here, the intermediate depth also presents increased growth like at the periphery, showing that increased carbon availability also allows cells to grow in deeper layers (Figure 4e,f).

We increased the thickness of the hemisphere to 4 mm to test how cells in lower layers will cope with increased light

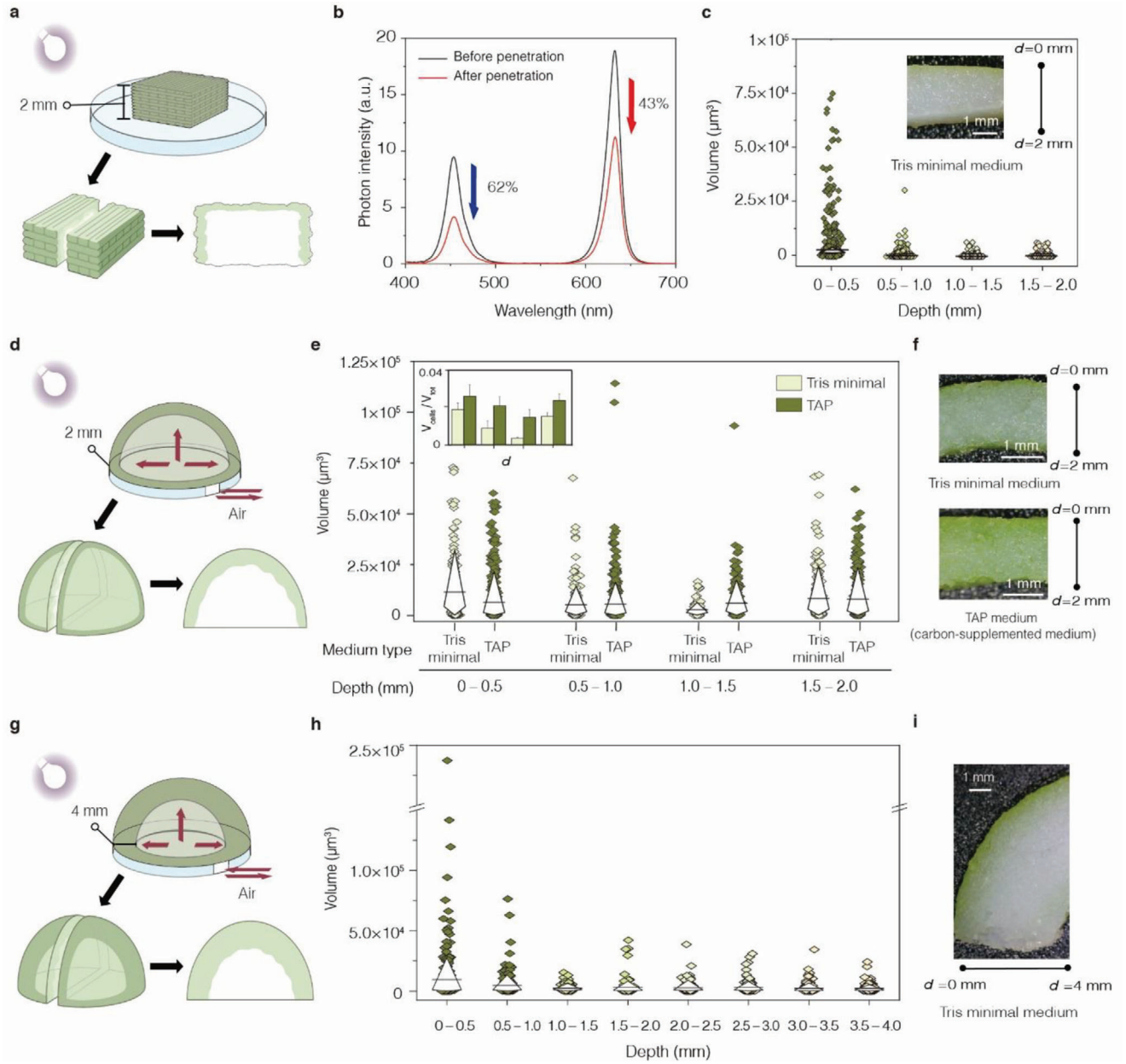

Figure 4. Exploring the limiting factors for growth of embedded *Chlamydomonas reinhardtii* (*C. reinhardtii*) cells in hydrogels. a) Experimental design using plate-shaped engineered living materials (ELMs) with 2 mm thickness. b) Attenuation of light after penetration through a 2 mm thick plate-shaped ELM containing algal cells, at 0 day old. c) Volume and spatial distribution for individual colonies embedded in 2 mm thick ELM-plates formulated with Tris minimal medium in relation to depth (d) from the top surface, after an incubation time of 14 days. A macroscopic image shows a typical cross-section of the ELM-plate used for measurement. d) Experimental design using 2 mm thick hollow ELM-hemispheres (external radius: 10 mm, internal radius: 8 mm), including an opening at the bottom allowing gas exchange of the hollow center with the environment. e) Volume distribution for individual colonies embedded in 2 mm thick hollow ELM-hemispheres in relation to depth and to medium composition, after an incubation time of 14 days. Inset: average volume fraction occupied by colonies (V_{cells}/V_{tot}) in 2 mm thick ELM-hemispheres in either Tris minimal medium (light green) or Tris-acetate-phosphorous (TAP) medium (dark green), depending on depth (d). For the *x* axis from left to right, each subsection indicates 0–0.5, 0.5–1.0, 1.0–1.5, and 1.5–2.0 mm. Error bars represent standard deviations from measurements of three separate hemispheres. f) Macroscopic images of 2 mm thick hollow ELM-hemispheres cross-section formulated with Tris minimal medium (top) and TAP medium (bottom) after an incubation time of 14 days. g) Designs using 4 mm thick hollow ELM-hemispheres (external radius: 10 mm, internal radius: 6 mm), including an opening at the bottom allowing gas exchange between the hollow center and the environment. h) Volume distribution of individual colonies embedded in 4 mm thick hollow ELM-hemispheres formulated with Tris minimal medium in relation to depth after an incubation time of 14 days. i) Macroscopic image of 4 mm thick hollow ELM-hemisphere cross-section formulated with Tris minimal medium after an incubation time of 14 days. In (c), (e), and (h), three samples were used for the distributions, diamond boxes indicate 10 and 90 percentile values, and horizontal lines in the middle indicate the mean.

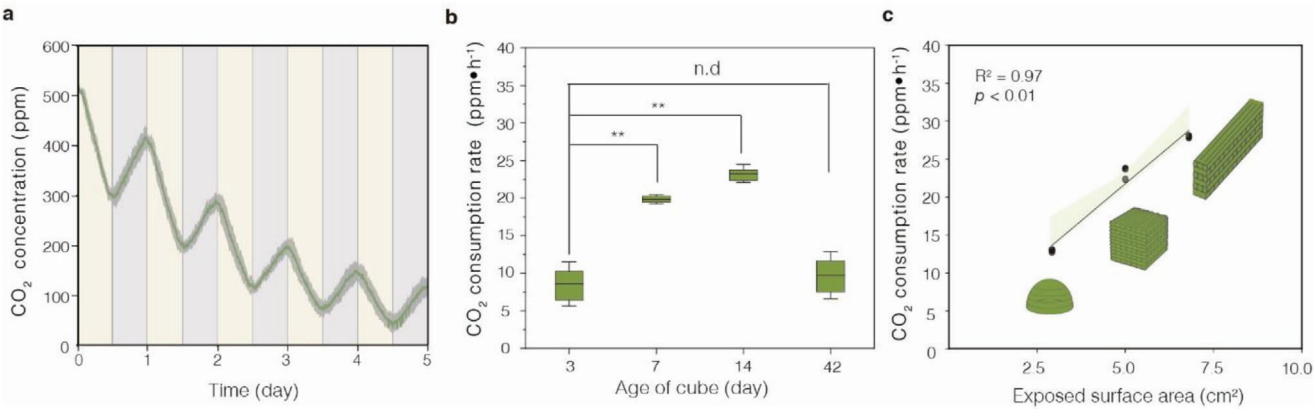

Figure 5. CO_2 consumption performance of photosynthetic living materials. a) 5-day time-course of average CO_2 concentration in a closed system containing a 7-day old engineered living materials (ELM) cube. The dark green line indicates the average from triplicate results, while shaded regions indicate standard deviation. A beige background represents a light intensity of 20 µmol m^{-2} s^{-1}, while a gray background represents darkness. b) Comparison of average CO_2 consumption rate of 3-, 7-, 14- and 42-day-old cubes during the first 12 h of illumination ($n = 3$, the box represents 25 and 75 percentile values, horizontal lines in the middle indicate mean, and whiskers extend to standard deviation). One-way (single factor) ANOVA with post-hoc Tukey's HSD was used for statistical analysis; n.d and ** indicate not significant and $p < 0.01$, respectively. c) Relationship between the exposed surface area of differently shaped ELMs and average CO_2 consumption rate ($n = 3$, the shaded areas indicate a pointwise 95% confidence interval on the fitted values). The bioprints with the shape of hemisphere ($r = 6.8$ mm; exposed surface area = 2.91 cm^2), cube (10 × 10 × 10 mm; exposed surface area = 5 cm^2), and cuboid (4 × 25 × 10 mm; exposed surface area = 6.8 cm^2) were 14 days old at the start of the experiment.

attenuation (Figure 4g). Despite the improved ambient CO_2 availability due to the hollow architecture and the hole allowing gas exchange, cell growth at the inner periphery was highly reduced compared to that at the outer periphery after 14 days of incubation (Figure 4h,i). Only ≈20% of initial light intensity at 453 nm (and ≈50% at 631 nm) can reach the inner space of a freshly printed 4 mm ELM-hemisphere (Figure S7, Supporting Information), which may further decrease with increased cell growth at the outer periphery. Light attenuation also similarly affects growth in 4 mm thick ELM-hemispheres with an additional carbon source (Figure S8, Supporting Information). Taken together, light permeability and CO_2 diffusion are key factors to consider in photosynthetic ELM designs, especially when microalgae are grown autotrophically.

2.4. CO_2 Consumption Performance of Photosynthetic Living Materials

The photosynthetic activity of microalgae embedded in ELMs can be indirectly monitored through consumption of ambient CO_2. The 1 cm^3 ELM-cubes were placed in a sealed glass container, illuminated with 12/12 h light/dark cycle at room temperature (≈22 °C) while the CO_2 concentration within the container was measured in real-time for 5 days. The measured CO_2 concentration decreased during light exposure and increased during periods of darkness (**Figure 5**a), implying that the embedded *C. reinhardtii* cells undergo photosynthesis and respiration while being illuminated, but mainly respiration while in darkness. Moreover, these measurements confirm that the cells endow photosynthetic capabilities to the ELM as a whole structure. Next, 3-, 7-, 14- and 42-day-old ELM-cubes were compared to test whether cell growth affects CO_2 consumption rate (Figure 5b). The 14-day-old cubes exhibited a statistically significant 2.7- and 1.2-fold higher CO_2 consumption performance than the 3-day-old and 7-day-old cubes ($p < 0.05$), respectively. Remarkably, 42-day old cubes still demonstrated photosynthetic activity. However, this longer incubation did not result in higher CO_2 capture performance, showing a similar level of CO_2 consumption rate compared to 3-day old cubes with lower cell numbers.

Since the colonies mostly grow at the periphery and cells in inner regions are less viable, a larger surface area might be helpful for the CO_2 consumption rate of ELMs. To test this, CO_2 consumption rate of three 14-day-old ELMs with different surface areas (hemisphere = 2.92 cm^2, cube = 5 cm^2, cuboid = 6.8 cm^2, excluding area facing the bottom) was measured while under 12 h of illumination. The CO_2 consumption rate increases linearly with the exposed surface area of the ELM (Figure 5c), with average CO_2 consumption rates of 12.9 ppm h^{-1} for the hemisphere, 23.3 ppm h^{-1} for the cube, and 28.0 ppm h^{-1} for the cuboid. The regression analysis revealed a high correlation between consumption rate and the ELM area with r^2 value of 0.96, showing that shapes with larger surface area are more beneficial for the photosynthetic activity of ELMs. Taken together, our data confirm our hypothesis that algal growth and metabolic activity in hydrogels can be modulated by the design of the ELM.

3. Discussion

Growth of cells within our microalgal ELMs showed a strong spatial dependence. Cells were found to dominate the outer periphery, especially when no additional carbon source (acetate) was provided. Limited gas diffusion and light attenuation caused reduced growth in deeper and/or central layers (depending on ELM architecture). The magnitude of light attenuation in deeper layers is dependent on the hydrogel thickness and is further attenuated by self-shading effects induced by colony growth in more mature ELMs. To better understand the geometrical parameters affecting microalgal growth, we prepared ELMs of different dimensions and shapes and found profound effects on *C. reinhardtii* cell

growth and productivity. In his 1917 book, Thompson argued that physical forces play a critical role in shaping biological forms.[35] We also found that shapes with a higher surface area showed a higher CO_2 consumption rate, likely due to a higher number of cells exposed to favorable light and gas diffusion.

Interestingly, also in fungal and bacterial ELMs, functionality was found to be strongly linked to micro and/or macroscopic structure and composition. For example, modulating sphericity of embedded *E. coli* colonies through tuning mechanical stiffness of hydrogel matrices led to higher protein productivity.[36] Taking advantage of 3D printing, lattice-structured hydrogels had improved mass transfer of nutrients, which increased yield of desired metabolic products from embedded yeast.[22] Similarly, recent work on the 3D shaping of mycelium-laden hydrogels also highlighted how branching cells can benefit from porous scaffolds that facilitate hyphal growth and interconnection, leading to regenerative 3D ELMs.[18,37]

For photosynthetic ELMs, a thin, plant-leaf like architecture may be beneficial for homogenous cell growth and resulting higher productivity per fixed volume. In plant leaves, the primary site of photosynthesis, is the palisade parenchyma, which is located below the upper epidermis of the leaf, which highlights the importance of light availability even in thin photosynthetic structures. Furthermore, gas exchange is regulated by stomata pores at the lower epidermis of plants. In this work, 3D printing allows us to be flexible in realizing beneficial shapes. A first attempt to steer cell growth was our hollow ELM-hemispheres which feature a small, though unregulated opening for gas exchange which visibly improved cell growth in the inner layers. Growth was further increased with providing an acetate source incorporated in the ELM, which shows that photosynthetic growth of autotroph ELMs would likely be even higher if CO_2 availability was further improved through features such as a porous architecture. However, improved gas exchange is in counterbalance with accelerated dehydration. This explains why the stomata in leaves open and close to improve gas exchange depending on plants' need while limiting dehydration. Leaves are also protected by a water-impenetrable wax-layer called cuticle, which is yet to be incorporated into our ELMs. Similar responsive additions to photosynthetic ELMs would likely benefit their longevity and photosynthetic productivity. Understanding microalgae growth within ELMs enables the development of fully controllable photosynthetic ELMs, which represent new solutions for oxygenating engineered tissues and organoids, and for energy production.

4. Conclusion

This work highlights that understanding the microbial response within 3D objects can help optimize ELM structures. A 3D printable hydrogel was developed whose structural integrity was further increased post-printing via cross-linking, allowing higher shaping capability. 3D mapping of microbial growth within ELMs is found to be key to identifying factors limiting cell growth, hence revealing ELM shape parameters (e.g., form and size) for improved ELM functionality. In photosynthetic ELMs, carbon source availability and light penetration are both found to be limiting factors for growth. Shaping ELMs in thin leaf-like structures, thereby maximizing surface to volume ratio, reduces the parts of ELMs with lower cell growth. Those plant-inspired structures could lead to high efficiency of photosynthesis in terms of CO_2 consumption and pave the way for new carbon capturing functional materials.

5. Experimental Section

Materials: Hutner's trace elements were purchased from Chlamydomonas Resource Center. Microcrystalline cellulose- and sodium carboxymethylcellulose-based thickener (MCG, VIVAPUR MCG 811 PV) was provided by JRS Pharma. Other chemical reagents used in this study (Tris base, acetic acid, ammonium chloride, magnesium sulfate heptahydrate, dipotassium phosphate, monopotassium phosphate, calcium chloride dihydrate, 37% hydrochloric acid solution, dried-powder of κ-carrageenan, sodium alginate from brown algae, and agar) were purchased from Sigma-Aldrich.

Strain and Culture Conditions: *Chlamydomonas reinhdardtii* CC-125 wild type mt(+) used in this study was obtained from Chlamydomonas Resource Center (USA). Microalgal cells were grown in a Tris minimal medium modified from previously,[38] (Tris: 2.42 g L^{-1}, salts solution (NH_4Cl: 5 g L^{-1}, $MgSO_4$ $7H_2O$: 4 g L^{-1}, and $CaCl_2$ $2H_2O$: 2 g L^{-1}) 25 mL L^{-1}, phosphate solution (K_2HPO_4 288 g L^{-1}, KH_2PO_4 144 g L^{-1}) 375 µL L^{-1}, Hutner's trace elements 1 mL L^{-1}; pH adjusted to 7.0 with hydrochloric acid) for growth under autotrophic conditions, or in TAP medium (identical to the Tris minimal medium except that the pH is adjusted to 7.0 with acetic acid) for growth under mixotrophic conditions. Liquid cultures with continuous air bubbling at room temperature (22 °C) were grown under a 12/12 light-dark cycle with an intensity of 20 µmol m^{-2} s^{-1} using PAR30S LEDs (Philips, The Netherlands).

Bioink Preparation: Hydrogel networks for bioprinting were formulated with either Tris minimal or TAP medium containing 1.5% (w/v) κ-carrageenan, 1.5% (w/v) sodium alginate, 1.5% (w/v) agar, and 3% (w/v) cellulose-based thickener. The thickener was dispersed into the media, mixed with a 1000 W Tristar MX-4828 hand blender at 16 000 rpm for 5 min, and rested for 15 min to ensure saturated swelling. Other hydrogel precursors were put individually with the following sequence: κ-carrageenan, sodium alginate, and agar. Each was mixed for 5 min and rested for 2 min, respectively. The resulting mixture with paste-like texture was autoclaved, conditioned at 30 °C for 2 days, and finely fragmented into granules with the blender for 5 min. Living microalgal cells grown in liquid cultures were harvested using a centrifuge at 3220 g for 5 min. Cell pellets were resuspended in 100 µL of Tris minimal media and transferred into the hydrogel matrix for bioink fabrication just prior to printing, resulting in a final concentration of 6.67×10^5 cells g^{-1}. The bio-ink was loaded to a 10-mL syringe and then degassed by centrifugation at 1690 g for 1 min.

Three-Dimensional Printing of Bioink: Three dimensional objects were fabricated with the following sequence: Computer-aided 3D (CAD) drawings, direct-ink writing, and Ca^{2+} cross-linking. The free online CAD program, TinkerCAD, was used to design 3D drawings of objects. Predesigned patterns and geometries with .stl file format were sliced using the Cura slicer engine in Repetier-Host (Hot-World GmbH & Co. KG., Germany) to generate G-code commands compatible with a modified Geetech A10 Pro 3D printer. Theoretical calculation of surface and volume of designs were also conducted with .stl file formats in the python console of FreeCAD.

A three-dimensional printer was modified by changing the filament hot-end part to a piston-based syringe pump and holder. The 10-mL syringe loaded with bioink was connected with a Metcal 18-gauge dispensing tip and fixed into syringe holders. The printing speed and travel speed were 20 and 200 mm s^{-1}, respectively, and every single layer of bioprints was deposited with a height of 0.5 mm. The resulting bioprints were immersed within varying concentrations of $CaCl_2$ solutions (0.1–0.5 M) for 5 and 60 min to cross-link polymers of hydrogels. After 3D printing, cell viability was checked with the fluorochrome SYTOX Green. The specific staining procedures are further described in the Supporting Information.

Bioprint Incubation: The 3D bioprints were subjected to two incubation conditions: air exposure and immersion in Tris minimal media. Air-exposed bioprints were enclosed in petri dishes sealed with parafilm. For immersion, each cube was placed into 10 mL of Tris minimal media in

6-well plates. All bioprints were maintained under 20 µmol m^{-2} s^{-1} at 12/12 h light/darkness interval using SQ100 LEDs (LUMERI, The Netherlands, the number of red and blue LED in a 5:1 ratio). In the light regime, 6.7 μmol m^{-2} s^{-1} at 453 nm and 13.3 μmol m^{-2} s^{-1} at 631 nm were measured with a LI-190R Quantum Sensor (LI-COR Biosciences, USA).

Light Intensity Measurement: To measure light absorption of bioprints with and without cells, both a CCS100 spectrometer (Thorlabs, Germany) and a LI-190R Quantum Sensor (LI-COR Biosciences, USA) were used. The sensor was placed directly under the petri dish containing the bioprint (2 mm thick plate-shaped ELMs, and 2 and 4 mm thick hollow ELM-hemispheres). Plastic plates without bioprints were used as blank.

Cell Imaging and Image Analysis: *Chlamydomonas reinhardtii* encapsulated within hydrogel networks were imaged using both a light microscope (Frederiksen Scientific, Denmark) and a confocal microscope (Nikon confocal A1R/SIM, Japan). For confocal microscopy, a laser with wavelength of 561 nm was set to excite chlorophyll and emission was collected with a band-pass filter at 595 ± 50 nm. The resonant scanning mirror was chosen for fast acquisition of real-time imaging to prevent desiccation induced hydrogel deformation. The obtained images were analyzed using the built-in functions of Fiji 2.9.0 to measure the size of cells or cell clusters. The detailed workflow of quantification using Fiji is given in the Supporting Information.

CO_2 Measurement: Individual bioprint inside a 60 mm diameter petri dish sealed with parafilm was placed inside a closed CO_2 measurement system. It was maintained under 20 µmol m^{-2} s^{-1}at 12/12 h light/dark cycle using Grow light LEDs (ABC-LED, The Netherlands, the number of red and blue LED in a 5:1 ratio). Information of the closed CO_2 measurement system is provided in the Supporting Information.

Rheology Test: The viscoelastic properties of hydrogel networks with and without microalgae were analyzed using circle plate-shaped prints (diameter: 20 mm, and height 2 mm) loaded onto a strain- and stress-controlled rheometer (Thermo Scientific HAAKE MARS III). Serrated plates of 20 mm diameter were used to prevent wall slip during the measurements with a gap height of 1 mm. Storage (G') and loss moduli (G'') were determined as a function of shear strain via oscillatory amplitude sweeps at a fixed frequency of 1 Hz with a sweep of strain (0.1–10 000%). The yield stress of the inks was determined by applying a stress-controlled deformation to the sample and measuring the resulting shear strain. The yield stress was measured using the tangent cross-over method in the log–log plots. The elastic recovery of the ink was measured using a time dependent oscillation–rotation–oscillation test. To simulate at rest behavior, amplitude sweep was performed at a low shear stress within the linear viscoelastic regime for 1 min followed by a high shear rate (10 s^{-1}) rotation for 30 s to simulate the time scales and stresses applied during printing. Subsequently, the recovery in elastic moduli over time was measured with the low amplitude oscillatory sweep for 2 min.

Bridging Ability of Ink: To assess the bridging ability, a triangular support structure was printed based on Kleger et al.,[27] followed by printing 12 spanning filaments across the support structure with a gap of 1.5 mm between them. To evaluate the sagging behavior, the deflection of the filaments was imaged using a VR-5000 Optical Profilometer (Keyence, Germany). The spanning length of the filaments was measured by analyzing the image from the profilometer via Fiji. The storage modulus of the ink after recovery obtained from recovery test was used to calculate the theoretical deflection. The experimental deflection was compared to the calculated theoretical deflection and extrapolated using fit factors.

Statistical Analysis: No data preprocessing has been conducted. Colony number (Figure 3d) in cube-shaped ELMs and CO_2 consumption data (Figure 5a,b) are shown as mean ± standard deviation. Average CO_2 consumption rates (in Figure 5b) were statistically analyzed with one-way (single factor) ANOVA with post-hoc Tukey's HSD on the

online statistical calculators https://astatsa.com

Supporting Information

Supporting Information is available from the Wiley Online Library or from the author.

Acknowledgements

The authors thank Eugeni (Zjenja) L. Doubrovski, Josine Beets, Kevin Kruger, and Marissa Ford for useful discussion, and Ramon van der Valk for technical support. J.-J. O. acknowledges funding by Basic Science Research Program through the National Research Foundation of Korea (NRF) funded by the Ministry of Education (grant number NRF-2022R1A6A3A03072013). This work was supported by the European Research Council (ERC starting grant no. 101042612).

Conflict of Interest

The authors declare no conflict of interest.

Data Availability Statement

The data that support the findings of this study are openly available in 4TU.ResearchData repository at https://10.4121/dbac218d-fca8-4c53-b39a-b7ebed3344ea.

Keywords

3D printing, CO_2 consumption, engineered living material, functional living surface, hydrogel, microalgae, spatial organization

Received: June 8, 2023
Revised: October 16, 2023
Published online:

[1] P. Gruber, J. Vincent, A. C. J. Vermeulen, T. Speck, *Built to Grow: Blending Architecture and Biology* (Eds.: B. Imhof, P. Gruber), Birkhäuser, Basel, **2016**.
[2] P. Q. Nguyen, N.-M. D. Courchesne, A. Duraj-Thatte, P. Praveschotinunt, N. S. Joshi, *Adv. Mater.* **2018**, *30*, 1704847.
[3] A. Rodrigo-Navarro, S. Sankaran, M. J. Dalby, A. Del Campo, M. Salmeron-Sanchez, *Nat. Rev. Mater.* **2021**, *6*, 1175.
[4] W. V. Srubar, III, *Trends Biotechnol.* **2021**, *39*, 574.
[5] B. Pabst, B. Pitts, E. Lauchnor, P. S. Stewart, *Antimicrob. Agents Chemother.* **2016**, *60*, 6294.
[6] H. Priks, T. Butelmann, A. Illarionov, T. G. Johnston, C. Fellin, T. Tamm, A. Nelson, R. Kumar, P.-J. Lahtvee, *ACS Appl. Bio Mater.* **2020**, *3*, 4273.
[7] S. Zhao, C. Guo, A. Kumarasena, F. G. Omenetto, D. L. Kaplan, *ACS Biomater. Sci. Eng.* **2019**, *5*, 4808.
[8] F. Krujatz, A. Lode, S. Brüggemeier, K. Schütz, J. Kramer, T. Bley, M. Gelinsky, J. Weber, *Eng. Life Sci.* **2015**, *15*, 678.
[9] A. Lode, F. Krujatz, S. Brüggemeier, M. Quade, K. Schütz, S. Knaack, J. Weber, T. Bley, M. Gelinsky, *Eng. Life Sci.* **2015**, *15*, 177.
[10] S. Malik, J. Hagopian, S. Mohite, C. Lintong, L. Stoffels, S. Giannakopoulos, R. Beckett, C. Leung, J. Ruiz, M. Cruz, B. Parker, *Global Challenges* **2020**, *4*, 1900064.
[11] C. Kwak, S. Young Ryu, H. Park, S. Lim, J. Yang, J. Kim, J. Hyung Kim, J. Lee, J. Lee, *J. Colloid Interface Sci.* **2021**, *582*, 81.
[12] F. He, Y. Ou, J. i. Liu, Q. Huang, B. Tang, F. Xin, J. Zhang, M. Jiang, S. u. Chen, Z. Yu, *Small* **2022**, *18*, 2104820.
[13] V. Kumar, M. S. Vlaskin, A. V. Grigorenko, *Trends Biotechnol.* **2021**, *39*, 1243.
[14] X. Chen, J. M. Lawrence, L. T. Wey, L. Schertel, Q. Jing, S. Vignolini, C. J. Howe, S. Kar-Narayan, J. Z. Zhang, *Nat. Mater.* **2022**, *21*, 811.
[15] S. Maharjan, J. Alva, C. Cámara, A. G. Rubio, D. Hernández, C. Delavaux, E. Correa, M. D. Romo, D. Bonilla, M. L. Santiago, *Matter* **2021**, *4*, 217.

[16] D. Datta, E. L. Weiss, D. Wangpraseurt, E. Hild, S. Chen, J. W. Golden, S. S. Golden, J. K. Pokorski, *Nat. Commun.* **2023**, *14*, 4742.
[17] S. Balasubramanian, K. Yu, A. S. Meyer, E. Karana, M.-E. Aubin-Tam, *Adv. Funct. Mater.* **2021**, *31*, 2011162.
[18] S. Gantenbein, E. Colucci, J. Käch, E. Trachsel, F. B. Coulter, P. A. Rühs, K. Masania, A. R. Studart, *Nat. Mater.* **2023**, *22*, 128.
[19] S. Balasubramanian, M.-E. Aubin-Tam, A. S. Meyer, *ACS Synth. Biol.* **2019**, *8*, 1564.
[20] O. Jeon, Y. u. B. Lee, H. Jeong, S. J. Lee, D. Wells, E. Alsberg, *Mater. Horiz.* **2019**, *6*, 1625.
[21] A. Lee, A. R. Hudson, D. J. Shiwarski, J. W. Tashman, T. J. Hinton, S. Yerneni, J. M. Bliley, P. G. Campbell, A. W. Feinberg, *Science* **2019**, *365*, 482;
[22] F. Qian, C. Zhu, J. M. Knipe, S. Ruelas, J. K. Stolaroff, J. R. Deotte, E. B. Duoss, C. M. Spadaccini, C. A. Henard, M. T. Guarnieri, S. E. Baker, *Nano Lett.* **2019**, *19*, 5829.
[23] J. L. Fredricks, H. Iyer, R. Mcdonald, J. Hsu, A. M. Jimenez, E. Roumeli, *J. Polym. Sci.* **2021**, *59*, 2878.
[24] N. Diamantides, C. Dugopolski, E. Blahut, S. Kennedy, L. J. Bonassar, *Biofabrication* **2019**, *11*, 045016.
[25] D. Petta, A. R. Armiento, D. Grijpma, M. Alini, D. Eglin, M. D'este, *Biofabrication* **2018**, *10*, 044104.
[26] D. Wangpraseurt, S. You, F. Azam, G. Jacucci, O. Gaidarenko, M. Hildebrand, M. Kühl, A. G. Smith, M. P. Davey, A. Smith, D. D. Deheyn, S. Chen, S. Vignolini, *Nat. Commun.* **2020**, *11*, 1748.
[27] N. Kleger, M. Cihova, K. Masania, A. R. Studart, J. F. Löffler, *Adv. Mater.* **2019**, *31*, 1903783.
[28] W. C. Ratcliff, M. D. Herron, K. Howell, J. T. Pentz, F. Rosenzweig, M. Travisano, *Nat. Commun.* **2013**, *4*, 2742.
[29] K. Iwasa, S. Murakami, *Physiol. Plant* **1968**, *21*, 1224.
[30] K. Iwasa, S. Murakami, *Acta Fac. Rerum Nat. Univ. Comenianae, Physiol. Plant.* **1969**, *22*, 43.
[31] T. Yoshitomi, S. Kaminaga, N. Sato, M. Toyoshima, T. Moriyama, K. Yoshimoto, *Plant Cell Physiol.* **2020**, *61*, 158.
[32] M. Al-Mossawi, H. Warren, P. J. Molino, P. Calvert, M. In Het Panhuis, *Mater. Adv.* **2021**, *2*, 1369.
[33] M. Sandmann, A. Garz, R. Menzel, *Botany* **2016**, *94*, 53.
[34] M. Vítová, K. Bisová, D. Umysová, M. Hlavová, S. Kawano, V. Zachleder, M. Čížková, *Planta* **2011**, *233*, 75.
[35] D. A. W. Thompson, *On Growth and Form*, Cambridge University Press, Cambridge, UK **1917**.
[36] S. Bhusari, S. Sankaran, A. Del Campo, *Adv. Sci.* **2022**, *9*, 2106026.
[37] A. R. Studart, K. Masania, *Nat. Mater.* **2023**, *22*, 16.
[38] D. S. Gorman, R. P. Levine, *Proc. Natl. Acad. Sci. U. S. A.* **1965**, *54*, 1665.